The Pure Silica Chabazite Molecular Spring: A Structural Study on Water Intrusion−Extrusion Processes

ARTICLE *in* THE JOURNAL OF PHYSICAL CHEMISTRY B · JULY 2008

Impact Factor: 3.3 · DOI: 10.1021/jp711889k · Source: PubMed

6 AUTHORS, INCLUDING:

Séverinne Rigolet
Institut de Science des Matériaux de Mulho…
85 PUBLICATIONS **764** CITATIONS

SEE PROFILE

J.-L. Paillaud
French National Centre for Scientific Resea…
122 PUBLICATIONS **1,352** CITATIONS

SEE PROFILE

Claire Marichal
Université de Haute-Alsace
79 PUBLICATIONS **663** CITATIONS

SEE PROFILE

THE JOURNAL OF PHYSICAL CHEMISTRY B

Article

Pure Silica Chabazite Molecular Spring: A Structural Study on Water Intrusion#Extrusion Processes

Mickae#l Trzpit, Se#verinne Rigolet, Jean-Louis Paillaud, Claire Marichal, Michel Soulard, and Joe#l Patarin

J. Phys. Chem. B, **2008**, 112 (24), 7257-7266 • DOI: 10.1021/jp711889k • Publication Date (Web): 21 May 2008

Pure Silica Chabazite Molecular Spring: A Structural Study on Water Intrusion−Extrusion Processes

Mickaël Trzpit, Séverinne Rigolet,* Jean-Louis Paillaud, Claire Marichal, Michel Soulard, and Joël Patarin

Laboratoire de Matériaux à Porosité Contrôlée, UMR CNRS 7016, ENSCMu, UHA, 3 rue Alfred Werner, 68093 Mulhouse Cedex, France

Received: December 19, 2007; Revised Manuscript Received: March 10, 2008

Water intrusion−extrusion isotherms performed at room temperature on hydrophobic pure silica chabazite show that the water−Si−CHA system displays real spring behavior. However, differences in pressure−volume diagrams are observed between the first and the other intrusion−extrusion cycles, indicating that some water molecules interact with the inorganic framework after the first intrusion. ^{29}Si and especially ^{1}H solid-state NMR showed the creation of new defect sites upon the intrusion−extrusion of water and the existence of two kinds of water molecules trapped in the supercage of Si−CHA: a first layer of water strongly hydrogen bonded with the silanols of the framework and a subsequent layer of liquidlike physisorbed water molecules undergoing interaction with the first layer. This hydrogen bonding scheme is also supported by X-ray powder diffraction.

Introduction

Zeolites, which are crystallized microporous solids with pore diameters lower than 1.4 nm, are involved in many industrial processes such as adsorption, catalysis, ion exchange, and membrane technology.[1] Pure silica zeolites (hydrophobic materials) have been recently proposed as porous matrices for water intrusion-based mechanical devices, leading to a new field of application concerning the energetics.[2–4] The phenomenon was based on the following principle: to spread a drop of a nonwetting liquid on the surface of a solid, a certain pressure must be applied. It is the same to make this liquid penetrate a porous matrix. During this stage, mechanical energy resulting from the compressive force can be converted into interfacial energy. On the microscopic scale, this phenomenon results in the breaking of intermolecular bonds in the liquid to create new bonds with the solid. By reducing the pressure, the system can evolve spontaneously by expelling the liquid out of the cavities of the solid (extrusion) with more or less significant hysteresis.[5] This process thus allows the storing and restoring of an important quantity of energy in a small volume. Indeed, although the interactions are rather weak (usually of the van der Waals type), they are acting over very large surface areas.

Such a property was shown for the first time by Eroshenko in 1996 on nonzeolitic porous solids with low-melting-point metals as nonwetting liquids.[6,7] In our research group, these studies were extended to systems made up of water and hydrophobic zeolites.[2–4] Depending on the zeolitic structure and its hydrophobic character, different behaviors illustrated by pressure−volume diagrams can be observed. Thus, silicalite-1, a pure silica MFI-type zeolite, acts as a spring; the intrusion−extrusion of water in this zeolite is completely reversible over several cycles. However, for a pure silica BEA-type zeolite whose structure consists of at least two polytypes, the phenomenon is nonreversible. The presence of defect sites at the interface of the two polytypes could explain the bumper behavior of such a solid.[3] Recently, we showed that the water-chabazite (Si−CHA) zeolite system is a new system capable to accumulating and restoring energy at a low pressure, which opens new applications for this porous solid.[8] However the water−Si−CHA system presents a small but reproducible decrease in the intruded pressure and volume between the first and the second cycles. Curiously for the others cycles, the intrusion and extrusion of water are completely similar.

The aim of this work is to gain a better understanding of the intrusion−extrusion process in the Si−CHA zeolite and, in particular, of the differences observed between the first and following intrusion−extrusion cycles. The Si−CHA samples, before and after the intrusion−extrusion of water, were fully characterized by thermal analysis, ^{29}Si and ^{1}H solid-state NMR spectroscopy, and Rietveld analysis.

Experimental Section

Sample Preparation. The Si−CHA samples were synthesized according to the procedure published by Diaz-Cabanas et al.[9] in a fluoride medium and using *N,N,N*-trimethyladamantammonium ($TMAda^+$) as a structure-directing agent. The starting gel of molar composition 1:0.5:0.5:3 SiO_2/TMAdaOH/HF/H_2O was introduced into a Teflon-lined stainless-steel autoclave and held at 150 °C for 90 h. After synthesis, the product was filtered, washed with distilled water, and dried at 60 °C overnight. The solid was then calcined at 600 °C under air to remove the organic template completely. The calcined sample will also be named the starting material in the present study.

Structure Analysis. For the structure analysis, the powder X-ray diffraction data (PXRD) of the starting material (calcined Si−CHA) and after four cycles of intrusion−extrusion of water were collected on a PANalytical MPD X'Pert Pro diffractometer in Debye−Scherrer geometry equipped with a capillary sample holder, a hybrid mirror monochromator (Cu $K\alpha_1$ radiation, $\lambda = 1.5406$ Å) that gives monochromatic parallel beam geometry, and an X'Celerator real-time multiple strip detector (active length = 2.12°(2θ)). The incident beam configuration was a ceramic Cu−LFF tube (45 kV, 35 mA), fixed divergence slit

* Corresponding author. E-mail: s.rigolet@uha.fr.

10.1021/jp711889k CCC: $40.75
Published on Web 05/21/2008

TABLE 1: Rietveld Refinement Data of the Starting and Intruded-Extruded Si−CHA Samples

chemical name	starting material Si−CHA	intruded−extruded Si−CHA
chemical formula (asymmetric unit)	$SiO_{2.029}$[a]	$SiO_{2.096}$[a]
calculated formula weight (g/mol)	60.55	61.62
space group	$R\bar{3}m$ (no. 166)	$R\bar{3}m$ (no. 166)
a (Å)	13.5407(1)	13.5438(1)
c (Å)	14.7612(1)	14.7587(1)
V (Å^3)	2343.90(2)	2344.55(2)
Z	36	36
density (calculated) (g cm^{-3})	1.544	1.571
number of contributing reflections	258	257
number of structural parameters	16	28
number of profile parameters	12	14
total number of restraints (Ow···O = 2.5(2) Å)[b]	0	18
total number of constraints	1[c]	0[c]
$R_p = \Sigma\{[y_o - y_c \times y_o - y_b/y_o]/\Sigma y_o - y_b\}$[d]	0.0525	0.0434
$wR_p = \{\Sigma[w \times (y_o - y_c) \times (y_o - y_b)/y_o]^2/\Sigma[w \times (y_o - y_b)^2]\}^{1/2}$[d]	0.0635	0.0488
wR_{exp}[e]	0.0593	0.0513
^eR_F	0.0697	0.0791
$R_F{}^2$[e]	0.0937	0.0955
χ^2[e]	1.148	0.904
largest diffraction peak and hole (e Å^{-3})	0.786, −1.148	0.686, −0.920

[a] In the chemical formulas, we consider that the sum of the oxygen atoms of the framework and the water molecules as listed in the Rietveld refinement did not take into account the scattering power of the hydrogen atoms of each water molecule. Consequently, the true number of water molecules should be about 25% lower than the s.o. factor refined for these oxygen atoms. [b] At the end of the refinement, the overall bond restraint weight was lowered to 1. [c] For the starting material, the thermal parameters of the framework oxygen atoms were constrained to be equal, but not for the intruded−extruded sample. [d] y_o, y_c, y_b, are y observed, y calculated, and y background, respectively. [e] The definitions of these residual values are given in ref 12.

(1/16°), hybrid monochromator, and antiscattering slit (1/2°). The diffracted beam with the X'Celerator configuration had an antiscattering shield and a Soller slit (0.02 rad). The grinded powder of the starting product (calcined Si−CHA) were introduced into a Mark tube made of special glass (no. 14, outside diameter 0.3 mm, Hilgenberg Gmbh), and then the capillary tube was mounted on a precise goniometric head that is screwed onto a rotary sample stage, where the spinning rate was 1 rotation/s. The powder pattern was collected at 295 K in the range of $8 < °(2\theta) < 90$, step = 0.008°, time/step = 3834 s). The same procedure was used for the intruded−extruded sample. The PXRD pattern of the starting material was indexed with the expected rhombohedral lattice for which the hexagonal set of the unit cell parameters (after refinement) is a = 13.5331(6) Å, c = 14.7508(6) Å, and V = 2339.61(18) Å^3 for the starting material and a = 13.5377(4) Å, c = 14.7513(4) Å, and V = 2341.26(12) Å^3 after four water intrusion−extrusion water cycles by the Visser ITO indexing routine[10] of the STOE WinXPow program package.[11] The figures of merit of this indexation were $F(30)$ = 344.7 and 362.3 in space group $R\bar{3}m$ (no. 166) for the starting material and after the intrusion−extrusion of water, respectively. The Rietveld refinements were performed with the complete patterns using the GSAS package.[12] The atomic coordinates of the framework atoms given by the structural commission of the IZA were used as the starting model for both analyses. All of the atoms were refined isotropically. Calculated Fourier difference maps allowed the location of some residual electronic densities that have been attributed to some occluded water molecules. Further details on the Rietveld refinement and crystallographic data are given in Table 1. The final atomic parameters are given in Table 2. In Table 3, bond distances and selected bond angles are reported. The final plots of the Rietveld refinements are given in Figures 1 and 2.

TG, SEM and N_2 Adsorption Analyses. Thermogravimetric (TG) and differential scanning calorimetry analyses (DSC) were carried out on a Setaram TG-DSC 111 apparatus under nitrogen−argon at a heating rate of 5 °C min^{-1} from 20 to 750 °C. Nitrogen adsorption isotherms were recorded using a Micromeritics ASAP 2010 apparatus. Prior to the adsorption measurements, the calcined samples were outgassed at 350 °C under vacuum. The size and the morphology of the crystals were determined by scanning electron microscopy (SEM) using a Philips XL 30 FEG microscope.

Solid-State NMR Spectroscopy. To identify the different types of protons present in the Si−CHA material, the samples under study must be dehydrated in order to remove the water that prevents the observation of the hydrogen species. The procedure allowing the elimination of physisorbed water but avoiding dehydroxylation reactions consists of holding the Si−CHA samples at 110 °C overnight under a reduced pressure of ∼3 Pa. The dehydrated samples are then transferred to a glovebox and packed in the 2.5 mm rotor under dry argon.

^{1}H ($I = {}^1/_2$) magic angle spinning (MAS) NMR experiments were performed at room temperature on a Bruker Avance II 400 spectrometer operating at B_0 = 9.4 T (Larmor frequency υ_0 = 400.13 MHz). Single-pulse experiments were recorded with a double-channel 2.5 mm Bruker MAS probe, a spinning frequency of 30 kHz, and a $^{\pi}/_2$ pulse duration of 4.8 μs. ^{1}H spin−lattice relaxation times (T_1) were measured with the inversion−recovery pulse sequence for all samples. Typically, 320 scans were recorded. ^{1}H double quantum (DQ) MAS NMR experiments were performed with a $^{\pi}/_2$ pulse length of 1.9 μs and a spinning frequency of 30 kHz. The duration of the excitation/reconversion of the double quantum coherences of the back-to-back (BABA) pulse sequence[13] were adjusted to two rotor periods (66.7 μs). ^{29}Si ($I = {}^1/_2$) MAS and ^{1}H−^{29}Si cross polarization magic angle spinning (CP-MAS) NMR spectra

TABLE 2: Atomic Coordinates, Site Occupancy, and Equivalent Isotropic Displacement Parameters for the Starting (Top) and the Intruded−Extruded (Down) Si−CHA Samples, With Standard Deviations in Parentheses

atoms	multiplicity and Wyckoff letters	s.o.f.	*x/a*	*y/b*	*z/c*	*U* [Å^2]
Si1	36i	1	0.4383(2)	0.1045(2)	0.7291(1)	0.0200(6)
O1	18h	1	0.5466(2)	0.0933(5)	0.7010(4)	0.021(1)[a]
O2	18f	1	1/3	0.0182(4)	2/3	0.021(1)[a]
O3	18h	1	0.4690(5)	0.2345(2)	0.7126(4)	0.021(1)[a]
O4	18g	1	0.4040(4)	0.0706(4)	5/6	0.021(1)[a]
Ow1	18h	0.059(6)	0.046(5)	0.091(9)	0.107(7)	0.12[b]
Si1	36i	1	0.4382(2)	0.1047(2)	0.7289(1)	0.0179(6)
O1	18h	1	0.5474(3)	0.0947(5)	0.7027(5)	0.018(3)
O2	18f	1	1/3	0.0188(5)	2/3	0.018(2)
O3	18h	1	0.4697(5)	0.23488(26)	0.7109(5)	0.018(3)
O4	18g	1	0.4037(4)	0.0704(4)	5/6	0.024(3)
Ow1	18h	0.022(4)	−0.327(4)	0.327(4)	0.307(8)	0.12
Ow2	36i	0.041(5)	0.445(4)	0.243(6)	0.281(5)	0.12
Ow3	18h	0.062(7)	0.294(4)	−0.294(4)	0.481(7)	0.12
Ow4	36i	0.012(6)	0.424(4)	0.167(5)	0.433(4)	0.12

[a] The thermal parameters of the framework oxygen atoms were constrained to be equal (with no constraint, the four values are close to each other, lying between 0.0175 and 0.019 with the same standard deviation). [b] Because of the strong correlation between the s.o.f. and the isotropic displacement parameters of the occluded water molecules, we fixed this parameter to the realistic value of 0.12.

TABLE 3: Bond lengths (Å) and Bond Angles (deg) for the Starting and the Intruded−Extruded Si−CHA Materials, With Standard Deviations in Parentheses

	starting material		
Si1	O1	1.603(6)	
	O2	1.604(3)	
	O3	1.612(5)	
	O4	1.606(2)	
	⟨Si−O⟩	1.606	
	starting material		
Si1	O1	O2	107.6(2)
	O1	O3	108.4(3)
	O1	O4	111.6(2)
	O2	O3	111.1(2)
	O2	O4	108.5(1)
	O3	O4	109.7(2)
	⟨O−Si−O⟩		109.5
	intruded−extruded material		
Si1	O1	1.598(3)	
	O2	1.601(3)	
	O3	1.615(3)	
	O4	1.610(3)	
	⟨Si−O⟩	1.606	
	intruded−extruded material		
Si1	O1	O2	108.8(3)
	O1	O3	107.5(4)
	O1	O4	110.8(3)
	O2	O3	110.7(4)
	O2	O4	108.4(3)
	O3	O4	110.6(3)
	⟨O−Si−O⟩		109.5

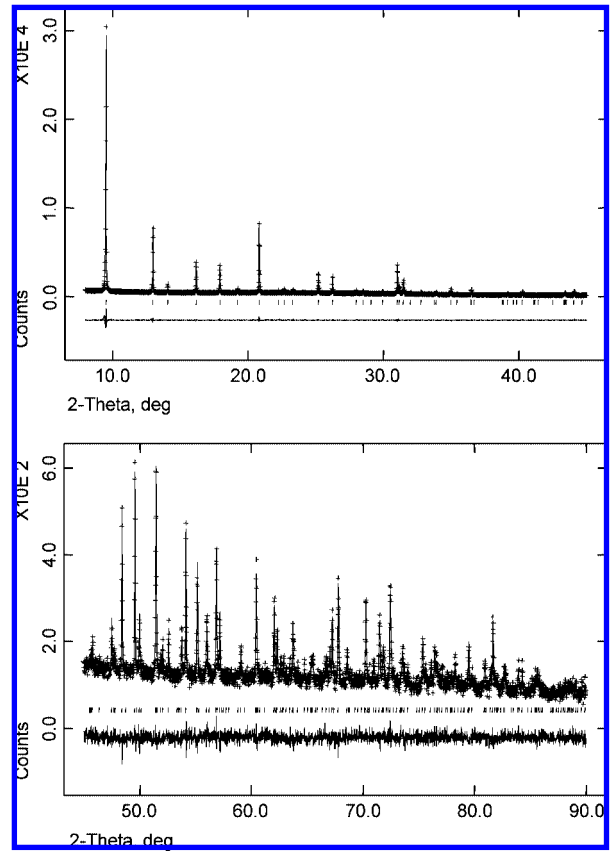

Figure 1. Rietveld plots of the starting Si−CHA material and experimental (+) and simulated (solid line) powder XRD patterns. Vertical ticks indicate the positions of the theoretical reflections for space group $R\bar{3}m$. The lowest trace is the difference plot.

were recorded, at room temperature, with a Bruker double-channel 7 mm probe on a Bruker Avance II 300 spectrometer operating at $B_0 = 7.1$ T (Larmor frequency υ_0 (^{29}Si) = 59.63 MHz and υ_0 (^{1}H) = 300.13 MHz). ^{29}Si single-pulse MAS NMR experiments were performed at a spinning frequency of 4 kHz, a $\pi/4$ pulse duration of 2 μs, and a 60 s recycling delay. These recording conditions ensure the quantitative determination of the proportions of the different Q_n Si species.[14] ^{1}H−^{29}Si CPMAS NMR experiments were acquired using a ramp for Hartmann−Hahn matching with a spinning frequency of 4 kHz, a ^{1}H $\pi/2$ pulse duration of 5.7 μs, and a contact time of 1 ms. The rf field strength used for ^{1}H decoupling was set to 62.5 kHz.

Chemical shifts reported thereafter are relative to tetramethylsilane for both ^{1}H and ^{29}Si nuclei. Decompositions of the spectra were performed using Dmfit software.[15]

Compressibility Tests. The intrusion−extrusion of water in Si−CHA samples was performed at room temperature using a modified mercury porosimeter (Micromeritics model autopore IV) with the procedure described in ref 8. The values of the intrusion (P_{int}) and extrusion (P_{ext}) pressures correspond to that of the half-volume total variation. Pressure is expressed in MPa,

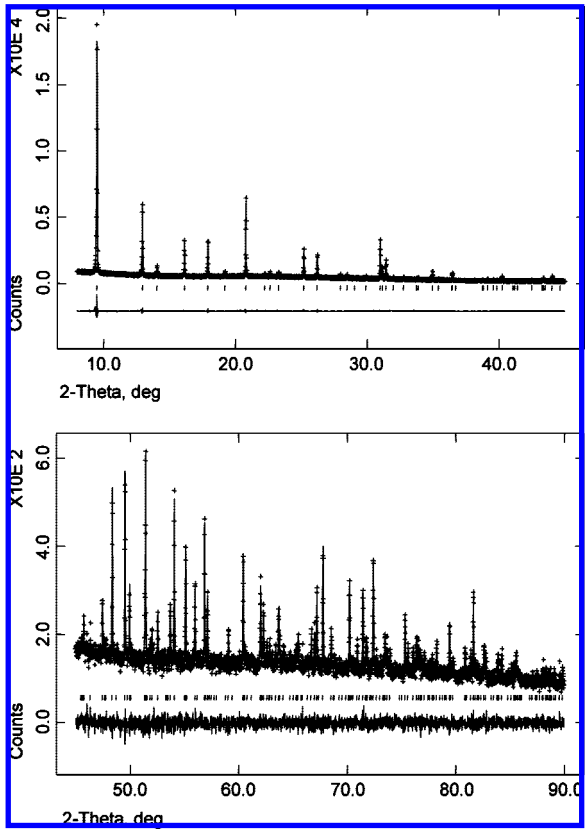

Figure 2. Rietveld plots of the intruded−extruded Si−CHA material and experimental (+) and simulated (solid line) powder XRD patterns. Vertical ticks indicate the positions of the theoretical reflections for space group $R\bar{3}m$. The lowest trace is the difference plot.

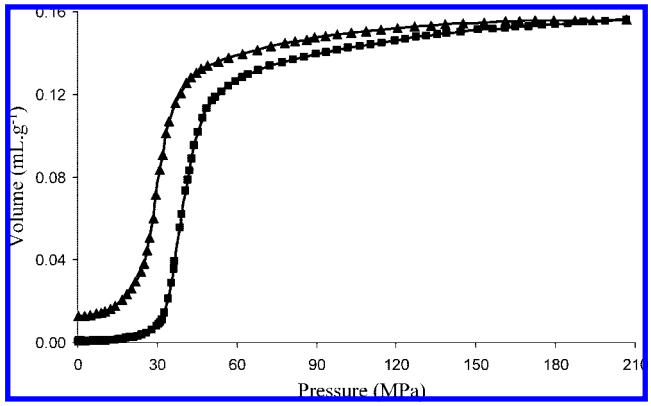

Figure 3. Pressure−volume diagrams of the water−Si−CHA system at room temperature: intrusion curve (■) and extrusion curve (▲).

and volume variation is expressed in milliliters per gram of anhydrous calcined zeolite. The experimental error is estimated to 1% in pressure and volume.

Results and Discussion

Pressure-Volume Isotherms. The Si−CHA pressure−volume diagram, at room temperature, is illustrated in Figure 3. Initially, the curves exhibit a linear part due to the compressibility of the condensed phases. When the pressure increases and the capillary pressure is reached (P_{int} = 42 MPa), water molecules penetrate into the pores of the solid. An important variation in volume is observed. Finally, after a complete filling of the pores, a classical compression step takes place. When the pressure is released, the phenomenon is reversible. However, the extrusion of water occurs at a lower pressure (P_{ext} = 30 MPa) showing hysteresis, and the extruded volume does not reach the initial one. Such phenomena can be due to the presence of hydrophilic defects sites created during the first intrusion of water, as will be shown below, and are in agreement with the experimental[16] and simulated[17] data of silicalite-1 samples displaying variable numbers of defects.

The water−Si−CHA system, as previously observed for the water−silicalite-1 system,[2] constitutes a real molecular spring. The intruded volume calculated with a water density of 1 is close to 0.16 mL g^{-1}, which is very different from that determined from N_2 adsorption measurements (i.e., 0.3 mL g^{-1}, Table 4). However, as shown by Desbiens et al. for silicalite-1, the water density in the MFI structure is ~0.6 .[18,19] By taking into account this correction for the Si−CHA sample, the intruded volume is thus totally consistent with the pore volume determined from nitrogen adsorption.

Pressure−volume diagrams at room temperature after one to four intrusion−extrusion cycles are fully described in a short communication,[8] and the experimental characteristics are summarized in Table 4. A small but reproducible difference is observed in pressure and in volume between the first and the second cycles whereas for the other cycles (cycles 2, 3, and 4), the intrusion curves on one side and the extrusion curves on the other side are completely superimposable. Depending on the Si−CHA samples, the variation in volume between the first and second cycles can reach 6%. This indicates that some water molecules after the first intrusion are not expelled when the pressure decreases. Indeed, after four water intrusion−extrusion cycles, when the Si−CHA sample is only dried at room temperature for 3 days, the $P-V$ diagram after one cycle corresponds to that of the second cycle of the starting material (Table 4, P_{int} = 37 MPa). However, when the same sample is calcined at 600 °C, the corresponding material displays a pressure−volume diagram after one cycle that is similar to that observed for cycle 1 of the starting material (Table 4, P_{int} = 42 MPa).

Common Characteristics of the Samples. Before or after the intrusion−extrusion of water, the crystals of Si−CHA exhibit cubic-shaped morphology with an average size of 3 × 3 × 3 μm^3 (Figure 4). In all cases, the symmetry of the structure remains unchanged. (See the structure analysis below.) The chemical analysis of the calcined, nonhydrated sample leads to the idealized unit cell formula $Si_{36}O_{72}$. Nitrogen adsorption measurements (curve not reported) performed at 77 K leads to a BET surface area of 850 $m^2 \cdot g$-L and a pore volume of 0.30 mL g^{-1} (Table 4).

Uncommon Characteristics of the Samples. Thermogravimetric analysis (Figure 5) was performed on the starting material (calcined Si−CHA) and the intruded−extruded (after four cycles) samples. Both samples were placed in a controlled saturated atmosphere of 85% water for 48 h. The amount of adsorbed water in the starting sample is approximately 2.5 wt % (3.1 water molecules per unit cell, weight loss spread out from 20 to 180 °C), whereas the TG curve of the intruded−extruded sample shows two main weight losses. The first one, from 50 to 180 °C (3 wt %, 3.7 water molecules per unit cell), corresponds to the removal of physisorbed water molecules, and the second one that occurs in two steps is observed between 180 and 700 °C (2.8 wt %, 3.5 water molecules per unit cell) could be due to water arising from dehydroxylation reactions. In all cases, the DSC curves (not reported) display a broad endothermic component.

TABLE 4: Characteristics of the Water−Si−CHA System

	calcined Si−CHA (starting material)				intruded−extruded Si−CHA sample [a]		intruded−extruded Si−CHA sample dried at room temperature for 3 days[a]	
	cycle 1	cycle 2	cycle 3	cycle 4	cycle 1	cycle 2	cycle 1	cycle 2
pore volume (mL g^{-1})[b]	0.30							
BET surface area ($m^2 \cdot g^{-1}$)[b]	850							
intrusion pressure (MPa)	41.6	36.9	37.0	36.9	42.0	37.0	36.8	37.0
extrusion pressure (MPa)	30.5	31.1	31.2	31.0	30.9	31.0	31.0	31.1
intruded volume (mL g^{-1})	0.157	0.148	0.148	0.148	0.157	0.148	0.148	0.148

[a] After four intrusion−extrusion cycles. [b] Determined from the nitrogen adsorption isotherm (77 K).

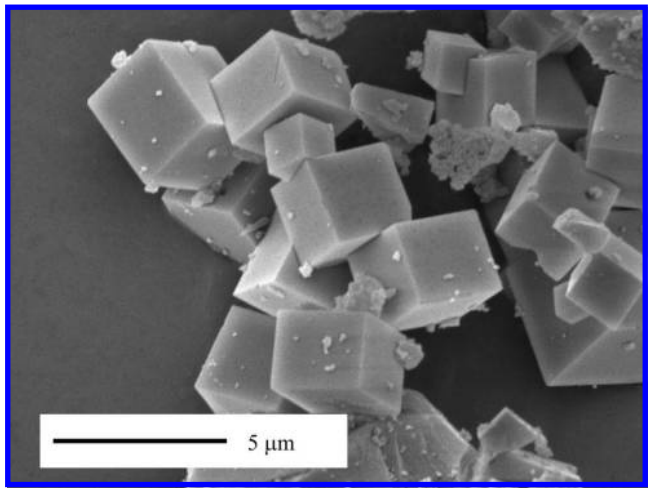

Figure 4. Micrographs of the Si−CHA sample.

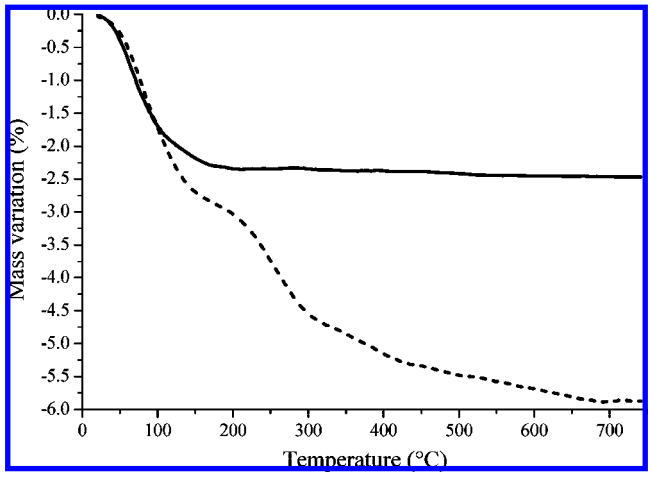

Figure 5. Thermogravimetric analysis of the starting material (−) and the intruded−extruded (after four cycles) sample (•••).

^{29}Si MAS NMR. The ^{29}Si MAS NMR spectra of both samples are reported in Figure 6. The spectrum of the starting material (calcined sample, Figure 6a) exhibits a very sharp, overwhelming resonance at −111.8 ppm corresponding to Q_4 groups Si−$(OSi)_4$.[14] A very small peak accounting for 4.3% of the total ^{29}Si signal is also detected at −102.4 ppm and can be assigned to Q_3 groups HO−Si−$(OSi)_3$.

After several water intrusion−extrusion cycles, those resonances are still observed in the ^{29}Si MAS NMR spectrum of the intruded−extruded sample (Figure 6b). Nevertheless, it is noteworthy that there is a 3.5% increase (Table 5) in the relative proportion of the resonance assigned to Q_3 species, indicating that some defects are created upon the intrusion−extrusion of water. Obviously, a small number of Si−O−Si bonds of the chabazite framework could be broken as a result of the imposed high water pressure. This is also in agreement with the significant broadening of the Q_4 resonance observed for this sample, indicating a decrease in the structural order of the inorganic framework. Such a result is in agreement with the decreased intrusion pressure observed after the first cycle.

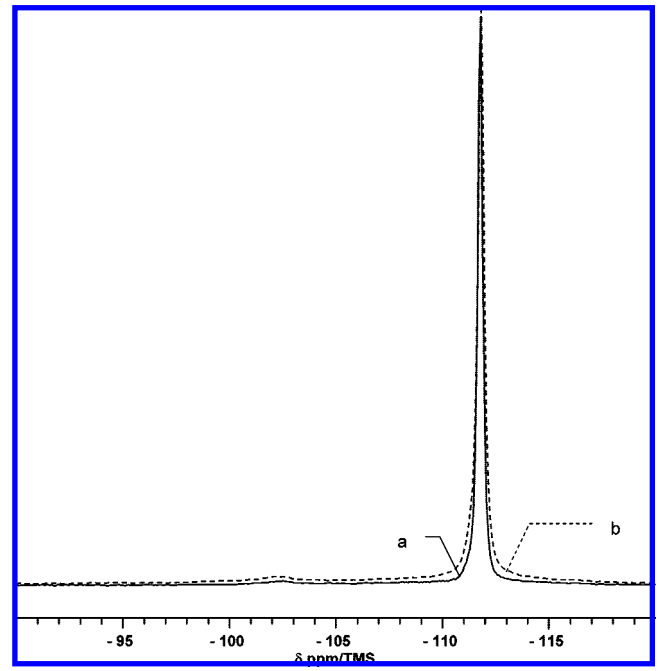

Figure 6. ^{29}Si MAS NMR spectra of the Si−CHA samples (a) before (starting material) and (b) after four water intrusion−extrusion cycles.

^{1}H−^{29}Si CPMAS NMR. The ^{1}H−^{29}Si CPMAS NMR spectra of the Si−CHA samples before and after water intrusion (Figure 7) were recorded with a short contact time (1 ms) in order to enhance the silicon atoms that bear protons. Indeed, such experiments show the presence of a resonance at −91.9 ppm corresponding to Q_2 species for both samples. In addition, the resonance assigned to the Q_3 species is broad and asymmetric, indicating the presence of at least three types of silanols. Two sharp resonances are observed at −101.2 and −102.4 ppm, a broader component appears at around −101 ppm (see the decomposition in Figure 7). ^{1}H−^{29}Si CPMAS NMR experiments are not quantitative, and deconvolution can be hazardous. Nevertheless, the relative number of Q_4 species reported in Table 5 decreases from 9.0 to 7.4% upon the intrusion−extrusion of water, indicating that the number of defects increase as already suggested by ^{29}Si MAS NMR.

^{1}H-MAS NMR. The ^{1}H MAS NMR spectra of the starting Si−CHA material before and after four water intrusion−extrusion cycles are displayed in Figure 8. The samples were dehydrated

TABLE 5: ^{29}Si Chemical Shift (ppm) and Amount of Silicate Species Estimated from MAS and CPMAS Spectra of the Si−CHA Samples before (Starting Sample) and after Four Water Intrusion−Extrusion Cycles

	calcined Si−CHA sample (starting material)			intrusion-extrusion Si−CHA sample		
	Si sites	δ	%	Si sites	δ	%
MAS	Q_3	−102.4	4.3	Q_3	−102.4	7.8
	Q_4	−111.7	95.7	Q_4	−111.8	92.2
	Q_2	−91.9		Q_2	−91.9	
CPMAS Tc = 1 ms	Q_3	−101.2	91.0[a]	Q_3	−101.0	92.6[a]
	Q_3'	−101.2		Q_3'	−101.3	
	Q_3''	−102.4		Q_3''	−102.4	
	Q_4	−111.7	9.0[a]	Q_4	−111.8	7.4[a]

[a] These values are reported for informational purposes only because ^{1}H−^{29}Si CPMAS NMR experiments are not quantitative.

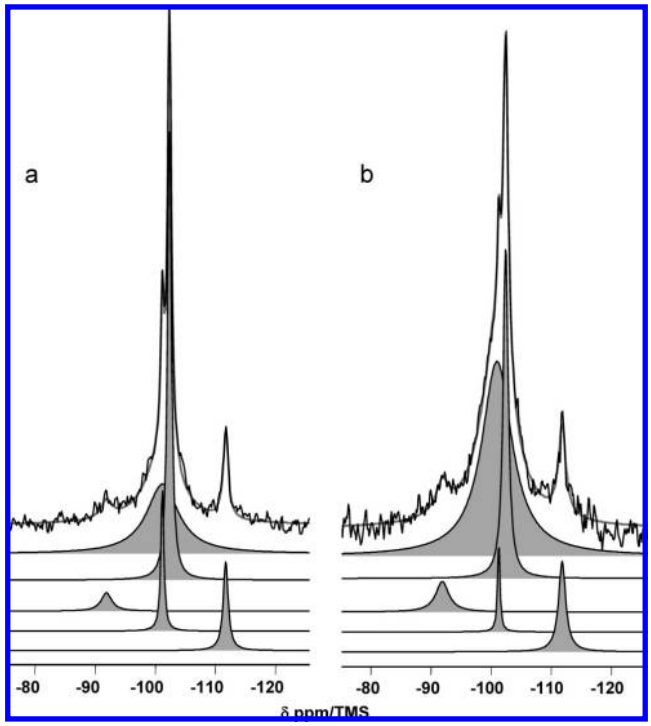

Figure 7. ^{1}H−^{29}Si MAS NMR spectra of the Si−CHA samples (a) before (starting material) and (b) after four water intrusion−extrusion cycles with their decomposition.

at 105 or 110 °C under reduced pressure for 12 h to remove the ^{1}H signal from physisorbed water molecules as much as possible. Note the good resolution of the spectra. Thus, thanks to decomposition with DMfit software,[15] six resonances at 0.9, 1.3, 1.9, 2.2, 3.2, and 4.7 ppm are observed for both samples that are dehydrated at 110 °C. According to their chemical shifts, they can be assigned to silanols (Si−OH) that are usually detected between 0 and 2 ppm, geminal silanols (Q_2 species) at 2.2 ppm, hydrogen-bonded water at 3.2 ppm, and liquidlike physisorbed water at 4.7 ppm.[20] Interestingly, in Figure 8b, the ^{1}H MAS NMR spectrum of the intruded−extruded chabazite sample reveals an additional relatively sharp, intense resonance at 0.1 ppm and a broad component in the 3−8 ppm range. The former could correspond to another kind of Si−OH silanol group created upon water intrusion, and the latter confirms the presence of water molecules trapped in the chabazite cage.

Complementary information can be deduced from these ^{1}H MAS NMR spectra. For the starting material (Figure 8a), the resonance at 1.9 ppm is decreasing when the water content is increasing, whereas the one at 3.2 ppm is increasing and for the most hydrated sample this line is shifted toward 4.7 ppm and dominates the spectrum. Consequently, resonances observed between 3 and 4.7 ppm correspond to silanols hydrogen bonded to water as already observed in mesoporous materials.[21] Note that the resonance at 1.3 ppm is not affected by the varying amount of water. Figure 8b shows the ^{1}H MAS NMR spectra of the intruded−extruded sample with variable amounts of water. In addition to the trends already observed before intrusion, the resonance at 0.1 ppm is stable upon dehydration/rehydration.

To gain further insight into the proton resonance assignments and the H−H proximities, ^{1}H single quantum/double quantum (DQ) MAS NMR spectra were recorded for both dehydrated (110 °C) samples. This experiment allows us to show pairs of dipolar coupled protons; the presence of a signal in the DQ spectrum indicates that two protons are in close proximity (<5 Å).[22] The result is shown in Figure 9. The DQ MAS NMR spectrum of the starting material (Figure 9a) shows that the ^{1}H resonance at 1.3 ppm exhibits a strong autocorrelation peak displayed on the dotted line diagonal of the 2D spectrum, indicating that there are at least two silanol groups in close proximity. Consequently, this resonance could correspond to clusters of silanols. On the contrary, the disappearance of the resonance at 1.9 ppm on the DQMAS spectrum implies that this resonance must correspond to isolated silanols. Autocorrelation is also observed for the resonance at 2.2 ppm, in agreement with the assignment[20,23] of this peak to geminal silanols (Q_2). Broad resonances displaying diagonal peaks are observed between 3 and 5 ppm, in agreement with the previous assignment of these resonances to hydrogen-bonded water molecules. It is worth mentioning that the ^{1}H chemical shift is strongly dependent upon the hydration state and the strength of the hydrogen bond can explain the observed dispersion of chemical shifts. Furthermore, the correlation between the peaks at 5.0 and 5.8 ppm (see black line in Figure 9) obviously corresponds to liquidlike physisorbed water,[21,24] indicating that a small amount of water is still present in this dehydrated compound.

After water intrusion, we already mentioned the appearance of a new resonance at 0.1 ppm that presents an autocorrelation on the DQ MAS NMR spectrum of the intruded−extruded sample (Figure 9b). This implies the proximity of at least two protons that could correspond either to neighboring silanols obtained after one siloxane Si−O−Si bond break (first hypothesis) or to a unique water molecule in a hydrophobic environment. Indeed, the ^{1}H chemical shift of monomeric H_2O in C_6D_6 was reported to be around 0.3 ppm.[25] Because calcined chabazite is a strongly hydrophobic zeolite material, the second hypothesis cannot be excluded.

To clarify this point, a 2D ^{1}H−^{29}Si CP HETCOR experiment (not reported), correlating the ^{1}H isotropic spectrum to neighboring ^{29}Si, was performed on the dehydrated (110 °C/~3 Pa) Si−CHA sample after four water intrusion−extrusion cycles. No correlation is observed at δ (^{1}H) = 0.1, which tends to prove

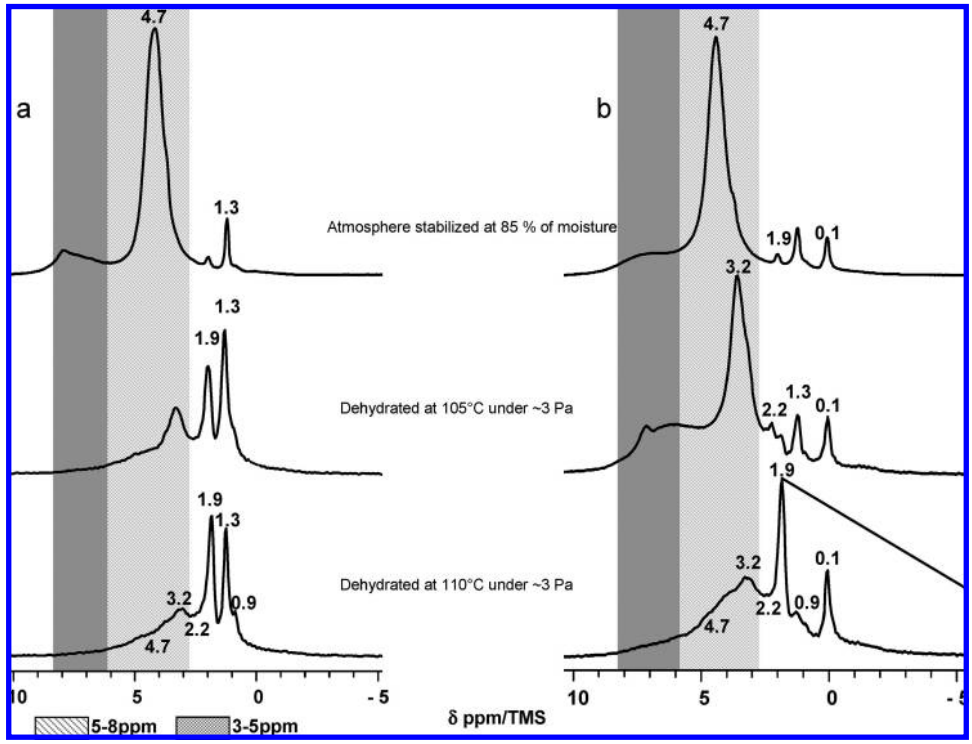

Figure 8. ^{1}H MAS NMR spectra of the Si−CHA samples dehydrated at 105 and 110 °C or hydrated under a controlled moisture atmosphere (a) before (starting material) and (b) after four water intrusion−extrusion cycles.

that this resonance cannot be assigned to the Si−O−H species. Furthermore, this ^{1}H resonance (0.1 ppm) was also observed in other systems (hydrophobic pure silicate zeolites) displaying different structures. Consequently, investigations are still in progress, and a comparative study will be undertaken to identify the nature of this signal.

Figure 9b also shows autocorrelation for the resonance at 1.3 ppm as already observed before intrusion. More interestingly, a correlation between this resonance and the one at 3.7 ppm is evidenced by this DQ MAS NMR experiment, indicating that water interacts preferentially with these clusters of silanols because no correlation between water and both resonances at 0.1 and 1.9 ppm is detected. Thus, one can conclude that these structural defects are responsible for the trapping of the strongly bonded water molecules as already reported in a previous study on silicalite-1.[16] Between 4 and 7 ppm, a broad region displaying off-diagonal correlations is observed because of the presence of hydrogen-bonded water molecules. In fact, from this NMR study, two populations of water can be distinguished: that of the first layer of water (3.7 ppm) strongly hydrogen bonded to the silanols at 1.3 ppm and that of the subsequent layer of liquid-like physisorbed water at about 5 ppm.

Structure Analysis. From the Rietveld refinements (Table 1), the long-range order of the Si−CHA framework remains intact even after the water treatment under pressure as suggested by the Si−O bond distances and the O−Si−O bond angles. In both cases, the unit cell parameters are similar (Table 1), and the average ⟨Si−O⟩ bonds (1.606 Å) and ⟨O−Si−O⟩ angles (109.5°) (Table 3) are characteristic of Si atoms in a perfect tetrahedrally coordinated environment. However, the formation of a small number of silanol nests inside the framework as suggested by the solid-state NMR study cannot be excluded. In fact, because of the high symmetry of the structure and the probable small amount of the possible siloxane Si−O−Si breaking, it was not possible to localize any defect during the Rietveld refinement. From this powder XRD study, the only advice that could indicate the eventual presence of defects in the framework is the higher isotropic thermal displacement factor of O4 in comparison with the three other framework oxygen sites in the case of the intruded−extruded sample (Table 2).

In the starting material, the computed difference Fourier maps allowed us to localize only one crystallographic site inside the so-called *chab* cavity or {3 [$4^{12}6^2$8^6]} cage for the occluded water molecules with an occupancy factor of about 0.059(6) (i.e., about 1 molecule of water per unit cell or *chab* cavity (Figure 10a)), which represents $^1/_3$ of the total water content as measured by TG analysis. The shortest distance between this water molecule and the framework oxygen atoms is Ow1···O1 = 4.1(7) Å. Note that other molecules of water could be present in the structure with undersized occupancy factors but their probable high disorder did not allow their accurate location. Anyway, the molecule of water located inside the *chab* cavity may be considered to be liquidlike physisorbed water and probably participates in the resonance at 4.7 ppm in the corresponding ^{1}H MAS NMR spectrum (Figure 8).

In opposition to the starting material, successive calculated difference Fourier maps during the Rietveld refinement allowed us to localize more than one crystallographic site for the occluded molecules of water in the intruded−extruded sample. Indeed, four crystallographic sites inside the *chab* cavity were found, giving rise to a water content of about three molecules of water (Figure 10b). No electronic density was found inside the small *d*6*r* cage, thus excluding the hypothesis of a unique water molecule entering this small *d*6*r* cage during the intrusion process. Fascinatingly, the located water molecules with characteristic O···O bond distances (Figure 10b and Table 6) form clusters with strong hydrogen bonds. It is possible to distinguish two kinds of water molecules. The first one, Ow2 and Ow4 strongly connected to the framework with Ow2···O2 = 2.72(8) Å, Ow2···O1 = 2.76(5) Å, Ow4···O1 = 2.45(6) Å, Ow4···O2 = 2.64(6) Å, and Ow4···O4 = 2.43(5) Å, are related to the

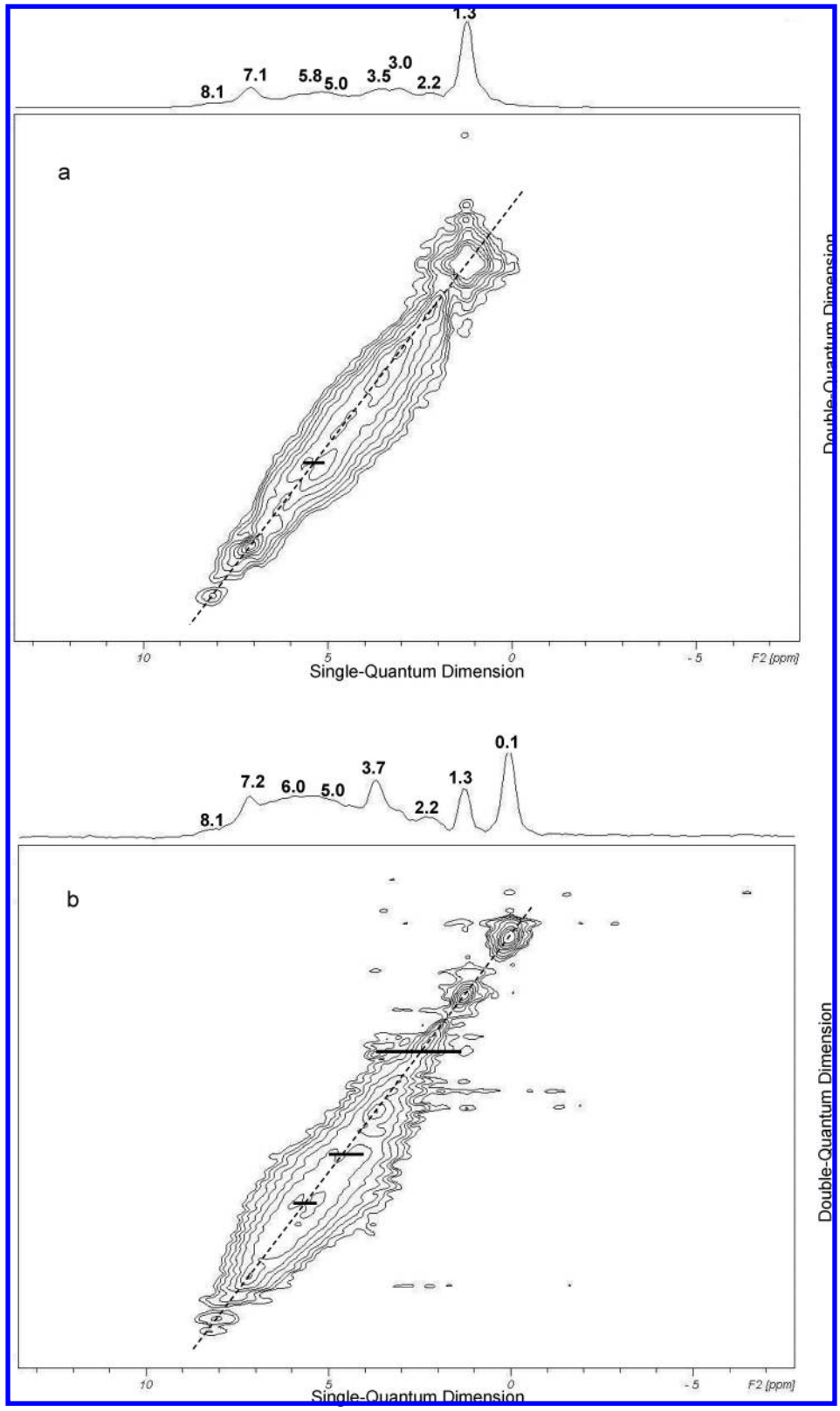

Figure 9. ^{1}H single quantum/double quantum (DQ) MAS NMR spectra of dehydrated (110 °C/~3 Pa) Si−CHA samples (a) before (starting material) and (b) after four water intrusion−extrusion cycles. The black line (−) correspond to the correlation between two different proton sites.

correlation observed by DQMAS NMR between the resonances located at 3.7 and 1.3 ppm. The second one, represented by Ow1 and Ow3, strongly interacts with Ow2 and Ow4 but not with the framework, and the shortest distances are Ow1···Ow2 = 2.5(1) Å, Ow1···Ow3 = 2.5(1) Å, and Ow3···Ow4 = 2.4(1) Å. With the number of Ow2 molecules per supercage being between 1.5 and 2, direct Ow2···Ow2 interaction is possible with the smallest distance of 2.6(1) Å (Figure 10b). This second layer of water molecules is also evidenced by the 3.7−5 ppm correlation (DQMAS NMR experiment, Figure 9b). It is worth noting that XRD and ^{1}H DQMAS NMR are in excellent agreement, offering a detailed view of the water behavior upon

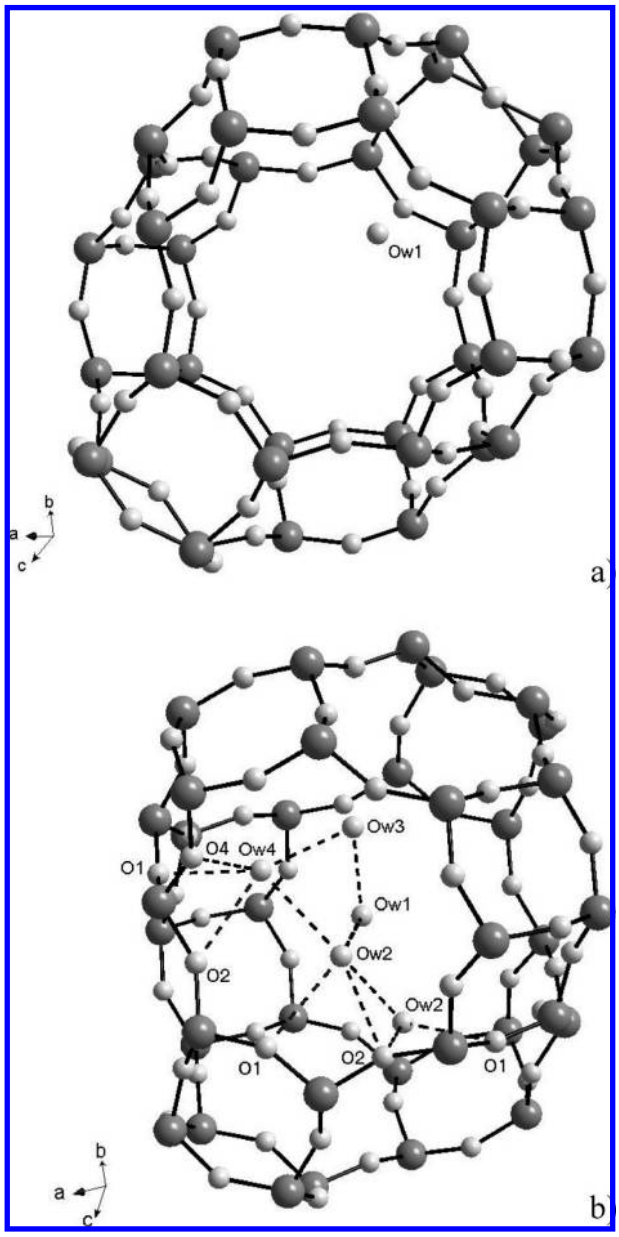

Figure 10. Central projection of a *chab* cavity of Si−CHA: (a) starting material and (b) intruded−extruded sample after four cycles.

intrusion. As already observed for the starting material, a probable high disorder did not permit the localization of the ~4 remaining occluded water molecules.

Conclusions

Solid-state NMR combined with XRD is a powerful tool for understanding the intrusion−extrusion process in the pure silica chabazite molecular spring.

In the starting calcined material, ^{29}Si and ^{1}H MAS NMR allowed us to quantify and identify different kinds of structural defects. In perfect agreement with the Rietveld refinement and TG data for this sample,^{1}H MAS NMR also shows that a small amount of water is still present in the supercage. Upon the first intrusion of water, NMR results indicate the creation of additional Si−OH groups. A small number of Si−O−Si bonds could be broken by the imposed high water pressure. When the pressure decreases, some water molecules are not expelled from the hydrophobic Si−CHA. The ^{1}H DQMAS NMR experiment showed that Si−OH clusters behave like a real water trap at the origin of two water populations, which is also perfectly illustrated by the structural refinement: a first layer of water strongly hydrogen bonded with the silanols of the framework and a subsequent layer of liquidlike physisorbed water molecules in interaction with the first layer. No further structural modification is observed during the second and the subsequent water intrusion−extrusion cycles.

TABLE 6: Possible Hydrogen Bond Schemes (Å) for the Intruded−Extruded Si−CHA Sample

Ow1	Ow2	2.5(1)
	Ow2	2.5(1)
	Ow2	2.71(6)
	Ow2	2.71(8)
	Ow2	2.74(7)
	Ow2	2.74(9)
	Ow2	2.78(9)
	Ow2	2.78(8)
	Ow2	2.81(9)
	Ow3	2.5(1)
	Ow3	2.5(1)
	Ow3	2.6(1)
Ow2	Ow4	2.42(9)
	O1	2.76(5)
	O2	2.72(8)
	Ow2	2.6(1)
	Ow4	2.6(1)
Ow3	Ow4	2.4(1)
Ow4	O1	2.45(6)
	O2	2.64(6)
	O4	2.43(5)

Acknowledgment. We thank Professor Alain H. Fuchs and his co-workers for fruitful discussions. This work was supported by the French Ministry of Education and Research (doctoral grant to M.T.) and the Agence National de la Recherche under contract no. BLANC06-3-144027.

References and Notes

(1) *Introduction to Zeolite Science and Practice*, 3rd ed.; Èejka, J., van Bekkum, H., Corma, A., Schüth, F., Eds.; Studies in Surface Science and Catalysis 168; Elsevier B.V.: Amsterdam, 2007; pp 525−1035.
(2) Eroshenko, V.; Regis, R. C.; Soulard, M.; Patarin, J. *J. Am. Chem. Soc.* **2001**, *123*, 8129–8130.
(3) Soulard, M.; Patarin, J.; Eroshenko, V.; Regis, R. C. In *Recent Advances in the Science and Technology of Zeolites and Related Materials: Proceedings of the 14th International Zeolite Conference*; Van Steen, E., Callanan, L., Claeys, M., Eds.; Studies in Surface Science and Catalysis 154; Elsevier B.V.: Amsterdam, 2004; pp 1830−1837.
(4) Eroshenko, V.; Regis, R. C.; Soulard, M.; Patarin, J. *C. R. Phys.* **2002**, *3*, 111–119.
(5) Denoyel, R.; Beurroies, I.; Lefevre, B. *J. Pet. Sci. Eng.* **2004**, *45*, 203–212.
(6) Eroshenko, V. Int. Pat. WO 9,618,040, 1996.
(7) Eroshenko, V. *Entropie* **1997**, *33*, 110–114.
(8) Trzpit, M.; Soulard, M.; Patarin, J. *Chem. Lett.* **2007**, *36*, 980–981.
(9) Diaz-Cabanas, M. J.; Barrett, P. A.; Camblor, M. A. *Chem. Commun.* **1998**, *17*, 1881–1882.
(10) Visser, J. W. *J. Appl. Crystallogr.* **1969**, *2*, 89–95.
(11) *STOE WinXPOW*, version 1.06; 1999.
(12) (a) Larson, A. C.; Von Dreele, R. B. General Structure Analysis System; Los Alamos National Laboratory Report LAUR 86-748, 2000. (b) Toby, B. H. *J. Appl. Crystallogr.* **2001**, *34*, 210–213.
(13) Feike, M.; Demco, D. E.; Graf, R.; Gottwald, J.; Hafner, S.; Spiess, H. W. *J. Magn. Reson. A* **1996**, *122*, 214–221.
(14) Engelhardt, G.; Michel, D. *High-Resolution Solid State NMR of Silicates and Zeolites*; John Wiley & Sons: Chichester, U.K., 1987.
(15) Massiot, D.; Fayon, F.; Capron, M.; King, I.; LeCalvé, S.; Alonso, B.; Durand, J.-O.; Bujoli, B.; Gan, Z.; Hoatson, G. *Magn. Reson. Chem.* **2002**, *40*, 70–76.
(16) Trzpit, M.; Soulard, M.; Patarin, J.; Desbiens, N.; Cailliez, F.; Boutin, A.; Demachy, I.; Fuchs, A. H. *Langmuir* **2007**, *23*, 10131.

(17) Cailliez, F.; Stirnemann, G.; Boutin, A.; Demachy, I.; Fuchs, A. H. accepted by *J. Phys. Chem. C.*

(18) Desbiens, N.; Demachy, I.; Fuchs, A.; Kirsch-Rodeschini, H.; Soulard, M.; Patarin, J. *Angew. Chem., Int. Ed.* **2005**, *44*, 5310–5313.

(19) Desbiens, N.; Boutin, A.; Demachy, I. *J. Phys. Chem. B* **2005**, *109*, 24071–24076.

(20) Burneau, A.; Gallas, J.-P. In *The Surface Properties of Silicas*; Legrand, A. P., Ed.; John Wiley & Sons: Chichester, U.K., 1998; pp 145−234.

(21) Trebosc, J.; Wiench, J. W.; Huh, S.; Lin, V. S.-Y.; Pruski, M. *J. Am. Chem. Soc.* **2005**, *127*, 3057–3068.

(22) Shantz, D. F.; Schmedt auf der Günne, J.; Koller, H.; Lobo, R. F. *J. Am. Chem. Soc.* **2000**, *122*, 6659.

(23) Dorémieux-Morin, C.; Heeribout, L.; Dumousseaux, C.; Fraissard, J.; Hommel, H.; Legrand, A. P. *J. Am. Chem. Soc.* **1996**, *118*, 13040–13045.

(24) Grünberg, B.; Emmler, T.; Gedat, E.; Shenderovich, I.; Findenegg, G. H.; Limbach, H.-H.; Buntkowsky, G. *Chem.—Eur. J.* **2004**, *10*, 5689–5696.

(25) Nakahara, M.; Wakai, C. *Chem. Lett.* **1992**, *21*, 809–810.

JP711889K